 CMES, vol.87, no.4, pp.327-354, 2012

Frequency Domain Analysis of Fluid-Solid Interaction Problems by Means of Iteratively Coupled Meshless Approaches

L. Godinho[1] **and D. Soares Jr.**[2]

Abstract: In this work, a coupling strategy between the Method of Fundamental Solutions (MFS) and the Kansa's Method (KM) for the analysis of fluid-solid interaction problems in the frequency domain is proposed. In this approach, the MFS is used to model the acoustic fluid medium, while KM accounts for the elastodynamic solid medium. The coupling between the two methods is performed iteratively, with independent discretizations being used for the two methods, without requiring matching between the boundary nodes along the solid-fluid interface. Two application examples, with single and multiple solid sub-domains, are presented, illustrating the behavior of the proposed approach.

Keywords: Acoustics; Elastodynamics; Iterative Coupling; Method of Fundamental Solutions; Kansa's Method; Frequency Domain Analysis.

1 Introduction

The investigation of interacting fluid and solid systems (e.g., fluids, such as air, water, lubricants, blood etc., coupled with structural elements, such as buildings, dams, offshore structures, mechanical components, pressure vessels, live organs etc.) is a research field of particular importance in engineering and science. In many cases, this interaction is quite expressive and must not be neglected, otherwise the related analyses may only represent a very crude approximation of the real model. This is particularly true in the case of a heavy fluid, such as water, interacting with a rather light solid, such as a membrane type structure. Up to now, a considerable amount of publications is available concerning the numerical modeling of coupled acoustic fluids and elastodynamic solids [Belytschko and Geers (1977); Mathews (1986); von Estorff and Antes (1991); Maman and Farhat (1995); Farhat,

[1] CICC, Department of Civil Engineering, University of Coimbra, 3030-788 Coimbra, Portugal.
[2] Structural Engineering Department, Federal University of Juiz de Fora, CEP 36036-330 Juiz de Fora, MG, Brazil

Lesoinne and LeTallec (1998); Lie, Yu and Zhao (2001); Park Felippa and Ohayon (2001); Czygan and von Estorff (2002); Lombard and Piraux (2004); Soares et al. (2007; 2010; 2011); Godinho, Amado-Mendes and Pereira (2011); among others], several of them even considering the coupling of different numerical procedures. However, few publications concentrate on the topic when meshless techniques are focused. Moreover, most coupling algorithms are formulated in a way that a coupled system of equations is established, which afterwards has to be solved using a standard direct solution scheme. Such a procedure leads to several problems with respect to efficiency, accuracy and flexibility. First, the coupled system of equations is usually rather large and it may no longer be able to make use of optimized solvers, due to the features of one of the involved sub-systems, which leads to rather expensive calculations with respect to computer time. Second, fluid and solid media usually have quite different physical properties, resulting in bad-conditioned coupled matrices when standard coupling procedures are considered, which may affect the accuracy of the methodology, providing misleading results. Third, the standard coupling methodology does not allow independent discretization for each sub-domain of the model, requiring matching nodes at common interfaces, which drastically affects the flexibility and versatility of the technique.

In order to evade these drawbacks, iterative coupling procedures have been recently presented, taking into account time domain fluid-solid interacting analyses, mostly considering boundary element - finite element coupled formulations [Soares et al. (2005; 2009); Warszawski, Soares and Mansur (2008)]. As it has been reported, iterative coupling approaches allow acoustic fluid and elastodynamic solid sub-domains to be analysed separately, leading to smaller and better-conditioned systems of equations (different solvers, suitable for each sub-domain, may be employed). Moreover, a small number of iterations is required for the algorithm to converge and the matrices related to the smaller governing systems of equations do not need to be treated (inverted, triangularized etc.) at each iterative step, providing an efficient methodology. As a matter of fact, in time domain analyses, iterative coupling procedures have been reported as effective techniques taking into account several wave propagation problems, being not restricted to fluid-solid applications [Soares von Estorff and Mansur (2004), Soares (2008), Soares(2012)], as well as not only to boundary element - finite element coupling procedures [Soares (2011)]. In non-transient problems, iterative coupling methodologies have also been reported as appropriate numerical tools, being several works presented on the topic, mostly considering potential and elastostatic problems [Lin (1996); Elleithy, Al-Gahtani and El-Gebeily (2001); Ya, Du and Hu (2006)].

In frequency domain analyses, although rarely, iterative coupling procedures have been reported in the literature, mostly considering acoustic-acoustic coupling [Ben-

amou and Despres (1997); Soares et al. (2012)]. As it has been reported, frequency domain wave propagation analyses usually give rise to ill-posed problems and, in these cases, the convergence of the iterative coupling algorithm can be either too slow or unachievable. This is the case in fluid-solid interacting models and, as discussed in this work, convergence can be hardly achieved if no special procedure is considered, especially if higher frequencies are focused. In order to deal with this ill-posed problem and ensure convergence of the iterative coupling algorithm, an optimal iterative procedure is adopted here, with optimal relaxation parameters being computed at each iterative step. As it is described along the paper, the introduction of these optimal relaxation parameters allows the iterative coupling technique to be very effective in the frequency domain, ensuring convergence at a low number of iterative steps.

In spite of the great success of the finite and boundary element methods as effective numerical tools for the solution of boundary-value problems on complex domains, there is still a growing interest in the development of new advanced methods. In this context, many meshless formulations are becoming popular due to their high adaptivity and low cost to prepare input data for numerical analysis, as well as mathematical simplicity and high accuracy and convergence rate features. In the present work, two distinct meshless methods are considered in order to numerically discretize the different sub-domains of the fluid-solid coupled model, namely: the Method of Fundamental Solutions (MFS) [Fairweather and Karageorghis (1998); Golberg and Chen (1999); Cho et al. (2004)], which is here applied to model the acoustic fluids; and the Radial Basis Functions (RBF) collocation method or the Kansa's Method (KM) [Kansa (1990a; 1990b)], which is here applied to numerically discretize the elastodynamic solids. The MFS is mathematically simple and is based on the prior knowledge of the Green's functions of the propagation subdomains. As with the Boundary Element Method, this limitation poses problems whenever inhomogeneous domains are to be analyzed, allowing, however, infinite media to be analyzed quite elegantly. The KM, on the other hand, follows a different approach by trying to reproduce the solution within a specific sub-domain as a linear combination of RBFs, being a closed domain formulation.

The paper is organized as follows: first, the governing equations of the physical problem are presented; then, the KM and the MFS are briefly discussed. In the sequence, the iterative coupling technique is described, including the mathematical derivation of the optimization methodology. At the end of the paper, numerical applications are presented, illustrating the accuracy, performance and potentialities of the proposed procedures.

2 Governing equations

In the frequency domain, the propagation of sound waves in a fluid medium, with sound speed υ, assuming null initial conditions, is governed by the Helmholtz equation:

$$\nabla^2 p + (\omega/\upsilon)^2 p = \gamma \text{ for } \mathbf{x} \in \Omega \tag{1}$$

where $p(\mathbf{x},\omega)$ is the acoustic pressure within the fluid and $\gamma(\mathbf{x},\omega)$ stands for domain sources. The boundary conditions for the problem can be given by:

$$p = \bar{p} \text{ for } \mathbf{x} \in \Gamma_p \tag{2a}$$

$$q = \nabla p \cdot \mathbf{n} = \bar{q} \text{ for } \mathbf{x} \in \Gamma_q \tag{2b}$$

where the prescribed values are indicated by over bars and $q(\mathbf{x},\omega)$ represents the fluxes along the boundary whose unit outward normal vector is represented by $\mathbf{n}$. The boundary of the model is denoted by Γ ($\Gamma = \Gamma_p \cup \Gamma_q$) and the domain by Ω. Equation (2a) stands for essential (or Dirichlet) boundary conditions and equation (2b) stands for natural (or Neumann) boundary conditions.

For elastodynamic models the governing equations are given by:

$$(\lambda + 2\mu)\nabla\nabla \cdot \mathbf{u} - \mu\, \nabla \times \nabla \times \mathbf{u} + \omega^2 \rho \mathbf{u} = \rho \mathbf{f} \text{ for } \mathbf{x} \in \Omega, \tag{3}$$

where λ and μ stand for the Lamé constants and ρ represents the density of the elastic medium. Further in equation (3), $\mathbf{u}(\mathbf{x},\omega)$ is the displacement vector and $\mathbf{f}(\mathbf{x},\omega)$ stands for domain forces. The boundary conditions for the problem are given by:

$$\mathbf{u} = \bar{\mathbf{u}} \text{ for } \mathbf{x} \in \Gamma_u, \tag{4a}$$

$$\boldsymbol{\tau} = \sigma \mathbf{n} = \bar{\boldsymbol{\tau}} \text{ for } \mathbf{x} \in \Gamma_\tau, \tag{4b}$$

where, once again, the prescribed values are indicated by over bars and $\boldsymbol{\tau}(\mathbf{x},\omega)$ represents the traction vector along the boundary ($\boldsymbol{\sigma}(\mathbf{x},\omega)$ stands for the stress tensor).

At the interface between the acoustic fluid and elastodynamic solid sub-domains, field continuity and equilibrium conditions are defined as:

$$u_N + 1/(\rho\omega^2)\, q = 0 \text{ for } \mathbf{x} \in \Gamma_i, \tag{5a}$$

$$\tau_N + p = 0 \text{ for } \mathbf{x} \in \Gamma_i, \tag{5b}$$

$$\tau_T = 0 \text{ for } \mathbf{x} \in \Gamma_i, \tag{5c}$$

where Γ_i stands for the common interface boundary and subscripts N and T represent normal and tangential components, respectively. It is important to observe that, in equations (5), the sign of the different sub-domain outward normal directions is taken into account (outward normal vectors on the same interface point are opposite for each sub-domain) and that ρ in equation (5a) stands for the mass density of the interacting acoustic fluid sub-domain.

3 Meshless modelling

In the sub-sections that follow, the numerical treatment of the previously presented governing equations is briefly discussed, taking into account the Kansa's Method (KM) and the Method of Fundamental Solutions (MFS), which are mathematically simple formulations. Here, the KM is employed to discretize the solid sub-domain, whereas the MFS is applied to model the fluid sub-domain. The MFS is based on the prior knowledge of the Green's functions of the model and it allows dealing with infinite media quite elegantly. The Kansa's Method, on the other hand, is a closed domain technique and it is based on the use of radial basis functions to describe the displacement fields within the solid sub-domains. In the next section, the coupling of these different methodologies is discussed, aiming to analyse a propagation domain with a limited zone modelled by the KM (designated as region Ω^a) and an external infinite host medium modelled by the MFS (region Ω^b).

3.1 Formulation of the Kansa's Method

In meshless methods relying on solution approximation with Radial Basis Functions, as it is the case of the Kansa's Method, the displacement $\mathbf{u}$, in equation (3), can be written as:

$$\mathbf{u}(\mathbf{x},\omega) = \sum_{n=1}^{N} \mathbf{a}_n(\omega)\,\varphi_n(\mathbf{x}) + \sum_{m=1}^{M} \mathbf{e}_m(\omega)\,P_m(\mathbf{x}) \tag{6}$$

where N and M represent the number of different basis functions used to build the approximation, $\varphi_n(\mathbf{x})$ and $P_m(\mathbf{x})$ stands for radial and polynomial basis functions, respectively, and $\mathbf{a}_n(\omega)$ and $\mathbf{e}_m(\omega)$ represent coefficients to be determined. Although the polynomial basis ensures consistency, it is possible to consider that the solution $\mathbf{u}$ is approximated by using only the contribution of RBFs (as for example in Tadeu, Godinho and Chen (2005)), so that the last term in equation (6) can be ignored. In this case, which is adopted in the context of this paper, a number of N collocation points is distributed throughout the domain and the boundary of the model; although not mandatory, here the collocation points are enforced to coincide

with the RBF centres. By applying this simplified version of approximation (6) to the governing equations (3)-(4), a system of $2N$ linear algebraic equations can be obtained, as is indicated below for 2D analysis (the sub-domains modelled by the KM are referred here by the superscript a):

$$\mathbf{H}^a\mathbf{a} = \mathbf{F}^a$$

or

$$\sum_{n=1}^{N}\left\{\begin{bmatrix} H^a_{xx} & H^a_{xy} \\ H^a_{yx} & H^a_{yy}\end{bmatrix}_{mn}\begin{bmatrix} a_x \\ a_y\end{bmatrix}_n\right\} = \begin{bmatrix} F^a_x \\ F^a_y\end{bmatrix}_m \text{ for each } \mathbf{x}^a_m, \tag{7}$$

where the entries of matrix $\mathbf{H}^a$ and vector $\mathbf{F}^a$are given by:

$$[H^a_{xx}]_{mn} = \frac{1}{2}(\lambda(1-\cos(2\theta))+(\lambda+2\mu)(1+\cos(2\theta)))(\partial\alpha^a_{mn}/\partial x)+(\mu\sin(2\theta))(\partial\alpha^a_{mn}/\partial y)$$

$$\left[H^a_{xy}\right]_{mn} = \frac{1}{2}(\lambda(1+\cos(2\theta))+(\lambda+2\mu)(1-\cos(2\theta)))(\partial\alpha^a_{mn}/\partial y)+(\mu\sin(2\theta))(\partial\alpha^a_{mn}/\partial x)$$

$$\left[H^a_{yx}\right]_{mn} = (\mu\cos(2\theta)))(\partial\alpha^a_{mn}/\partial y)-(\mu\sin(2\theta))(\partial\alpha^a_{mn}/\partial x)$$

$$\left[H^a_{yy}\right]_{mn} = (\mu\sin(2\theta)))(\partial\alpha^a_{mn}/\partial y)+(\mu\cos(2\theta))(\partial\alpha^a_{mn}/\partial x), \text{ for } \mathbf{x}^a_m \in \Gamma^a_\tau; \tag{8a}$$

$$[H^a_{xx}]_{mn} = \left[H^a_{yy}\right]_{mn} = \alpha^a_{mn}, \quad \left[H^a_{xy}\right]_{mn} = \left[H^a_{yx}\right]_{mn} = 0, \text{ for } \mathbf{x}^a_m \in \Gamma^a_u; \tag{8b}$$

$$[H^a_{xx}]_{mn} = (\lambda+2\mu)(\partial^2\alpha^a_{mn}/\partial x^2)+\mu\,(\partial^2\alpha^a_{mn}/\partial y^2)+\rho\omega^2(\alpha^a_{mn})$$

$$\left[H^a_{xy}\right]_{mn} = \left[H^a_{yx}\right]_{mn} = (\lambda+\mu)(\partial^2\alpha^a_{mn}/\partial x\partial y)$$

$$\left[H^a_{yy}\right]_{mn} = (\lambda+2\mu)(\partial^2\alpha^a_{mn}/\partial y^2)+\mu\,(\partial^2\alpha^a_{mn}/\partial x^2)+\rho\omega^2(\alpha^a_{mn}), \text{ for } \mathbf{x}^a_m \in \Omega^a; \tag{8c}$$

$$[F_x^a]_m = \bar{\tau}_{N_m}^a, \quad \left[F_y^a\right]_m = \bar{\tau}_{T_m}^a, \text{ for } \mathbf{x}_m^a \in \Gamma_\tau^a; \tag{9a}$$

$$[F_x^a]_m = \bar{u}_{x_m}^a, \quad \left[F_y^a\right]_m = \bar{u}_{y_m}^a, \text{ for } \mathbf{x}_m^a \in \Gamma_u^a; \tag{9b}$$

$$[F_x^a]_m = \rho \mathrm{f}_{x_m}^a, \quad \left[F_y^a\right]_m = \rho \mathrm{f}_{y_m}^a, \text{ for } \mathbf{x}_m^a \in \Omega^a. \tag{9c}$$

In equations (8)-(9), the following notation is adopted $V_m^a = V(\mathbf{x}_m^a, \omega)$, θ stands for the boundary normal angle at point $\mathbf{x}_m^a$, and the term α_{mn}^a is given considering multiquadric (MQ) radial basis functions, i.e.:

$$\alpha_{mn}^a = \sqrt{(x_m^a - x_n^a)^2 + (y_m^a - y_n^a)^2 + c^2} \tag{10}$$

where c is the shape parameter of MQ. It is worth noting that the MQ RBF is probably the most widely used RBF, and it is also the most usual choice for the KM. One known issue of using Kansa's Method with the MQ RBFs is the adequate definition of the free parameter c. In fact, c must be previously estimated and can significantly influence the condition-number of the system matrix and the accuracy of the results. Many works have analyzed strategies for the definition of an optimal shape parameter [Kansa and Hon (2000); Fasshauer and Zhang (2007); Sarra and Sturgill (2009); etc.], but the definition of an efficient and accurate methodology for the estimation of c is still an open discussion. Once the system of equations (7) is solved (i.e., vector $\mathbf{a}$ is computed), the approximate solution at any point of interest (and not only on nodal points – which is important when considering non-matching nodes in coupled analysis) can be obtained using the simplified form of equation (6), as described below:

$$\mathbf{u}_m^a = \sum_{n=1}^{N} \mathbf{a}_n \alpha_{mn}^a \text{ for } \mathbf{x}_m^a \in \Gamma^a \cup \Omega^a. \tag{11}$$

3.2 Formulation of the Method of Fundamental Solutions

In the MFS, the solution p is approximated by a linear combination of fundamental solutions centred on N_s virtual sources, placed outside the domain of interest to avoid singularities in the response, at $\mathbf{x}^s$:

$$p(\mathbf{x}, \omega) = \sum_{n=1}^{N_s} b_n(\omega)\, G(\mathbf{x}, \mathbf{x}_n^s, \omega) + \hat{\gamma}(\mathbf{x}, \omega) \tag{12}$$

where $G(\mathbf{x}, \mathbf{x}_n^s, \omega)$ stands for the Green's function of the model, $\hat{\gamma}(\mathbf{x}, \omega)$ is related to domain source terms and $b_n(\omega)$ represents coefficients to be determined.

By applying approximation (12) to the model, a system of algebraic equations can be obtained, as is indicated below (the sub-domains modelled by the MFS are referred here by the superscript b):

$$\mathbf{H}^b\mathbf{b} = \mathbf{F}^b \text{ or } \sum_{n=1}^{N}\left\{[H^b]_{mn}[b]_n\right\} = [F^b]_m \text{ for each } \mathbf{x}_m^b, \tag{13}$$

where the entries of matrix $\mathbf{H}^b$ and vector $\mathbf{F}^b$are given by:

$$[H^b]_{mn} = \frac{\mathrm{i}\omega}{4\upsilon^b}\mathrm{H}_1^{(2)}\left(\frac{\omega}{\upsilon^b}\beta_{mn}^b\right)\frac{\partial\beta_{mn}^b}{\partial\mathbf{n}_m^b}, \text{ for } \mathbf{x}_m^b \in \Gamma_q^b; \tag{14a}$$

$$[H^b]_{mn} = -\frac{\mathrm{i}}{4}\mathrm{H}_0^{(2)}\left(\frac{\omega}{\upsilon^b}\beta_{mn}^b\right), \text{ for } \mathbf{x}_m^b \in \Gamma_p^b; \tag{14b}$$

$$[F^b]_m = -\frac{\partial\hat{\gamma}_m^b}{\partial\mathbf{n}_m^b} + \bar{q}_m^b, \text{ for } \mathbf{x}_m^b \in \Gamma_q^b; \tag{15a}$$

$$[F^b]_m = -\hat{\gamma}_m^b + \bar{p}_m^b, \text{ for } \mathbf{x}_m^b \in \Gamma_p^b; \tag{15b}$$

and $\mathrm{H}_0^{(2)}$ and $\mathrm{H}_1^{(2)}$ stand for second type Hankel's functions of order 0 and 1, respectively.

In the deduction of equations (14)-(15), the 2D Green's function expression is considered (i.e., $G(\mathbf{x}_m, \mathbf{x}_n^s, \omega) = -(\mathrm{i}/4)\mathrm{H}_0^{(2)}((\omega/\upsilon^b)\beta_{mn}^b)$) and the term β_{mn}^b is given by:

$$\beta_{mn}^b = \sqrt{(x_m^b - x_n^s)^2 + (y_m^b - y_n^s)^2} \tag{16}$$

where $\mathbf{x}_n^s$ stands for the location of the virtual sources.

Once the system of equations (13) is solved (i.e., vector $\mathbf{b}$ is computed), the approximate solution at any point of interest can be obtained using definition (12), as described below:

$$p_m^b = -\frac{\mathrm{i}}{4}\sum_{n=1}^{N_s} b_n \mathrm{H}_0^{(2)}\left(\frac{\omega}{\upsilon^b}\beta_{mn}^b\right) + \hat{\gamma}_m^b \text{ for } \mathbf{x}_m^b \in \Gamma^b \cup \Omega^b. \tag{17}$$

4 Coupling procedure

In order to enable the coupling between the fluid (MFS) and solid (KM) parts of the model, an iterative procedure is employed here, which performs a successive renewal of the relevant variables at the fluid-solid interface. The proposed approach

is based on the imposition of prescribed fluxes at the fluid sub-domain and of prescribed tractions at the solid sub-domain. Since the two sub-domains are analyzed separately, the relevant systems of equations are formed independently, before the iterative process starts, and are kept constant for each frequency along the iterative process. The separate treatment of the two subdomains allows independent discretizations to be used on both parts, without any special requirement of matching nodes along the common interface. Thus, the coupling algorithm can be presented for a generic case, in which the interface nodes may not match, allowing exploiting this benefit of the iterative coupling formulation.

To ensure and/or to speed up convergence, a relaxation parameter ϕ is introduced in the iterative coupling algorithm. The effectiveness of the iterative process is strongly related to the selection of this relaxation parameter, since an inappropriate selection for ϕ can significantly increase the number of iterations in the analysis or, even worse, make convergence unfeasible. At the end of the section, an optimal relaxation parameter is calculated, taking into account the coupled fluid-solid frequency-domain formulation.

4.1 Iterative coupling algorithm

Initially, in the k^{th} iterative step of the MFS-KM acoustic-elastodynamic coupling, the MFS sub-domain is analyzed and vector $\mathbf{b}^{(k)}$ (the superscript k stands for the iterative step) is computed according to equation (13), considering expressions (14a) and (15a) for the entries of matrix $\mathbf{H}^b$ and vector $\mathbf{F}^b$, respectively, related to the common interfaces. Once vector $\mathbf{b}^{(k)}$ is computed, the pressures at the interface nodes of the KM sub-domains can be evaluated as follows (see also equation (17)):

$$\mathbf{P}^{a(k)} = \mathbf{B}^a \mathbf{b}^{(k)} + \mathbf{S}^a \tag{18}$$

where the entries of matrix $\mathbf{B}^a$ and vector $\mathbf{S}^a$ (which do not depend on the iterative step and can be computed just once for each frequency) are given by:

$$B^a_{mn} = -\frac{\mathrm{i}}{4}\mathrm{H}_0^{(2)}\left(\left(\omega/\upsilon^b\right)\beta^a_{mn}\right) \text{ and } S^a_m = \hat{\gamma}^a_m \tag{19}$$

The computed pressures can then be applied as prescribed Neumann boundary conditions for the sub-domains modelled by the KM (see equations (5b-c)), and vector $\mathbf{a}^{(k)}$ can be calculated, according to equation (7), considering expressions (8a) and (9a) for the entries of matrix $\mathbf{H}^a$ and vector $\mathbf{F}^a$, respectively, related to the common interfaces. Once vector $\mathbf{a}^{(k)}$ is computed, the normal displacements at the interface nodes of the MFS sub-domains can be evaluated as follows (see equation (11)):

$$\mathbf{U}_N^{b\,(k+\phi)} = \mathbf{A}^b \mathbf{a}^{(k)}, \tag{20}$$

where the entries of matrix $\mathbf{A}^b$ (which also do not depend on the iterative step) are given by:

$$\mathbf{A}^b_{mn} = [\cos(\theta) \;\; \sin(\theta)]\, \alpha^b_{mn}, \tag{21}$$

in which θ stands for the interface normal angle at point $\mathbf{x}^b_m$.

In the sequence, a relaxation parameter ϕ is introduced in order to ensure and/or to speed up convergence, such that:

$$\mathbf{U}_N^{b\,(k+1)} = (\phi)\mathbf{U}_N^{b\,(k+\phi)} + (1-\phi)\mathbf{U}_N^{b\,(k)}. \tag{22}$$

The computed normal displacements can then be applied as prescribed Neumann boundary conditions for the sub-domains modelled by the MFS (see equation (5a)), which are once again analysed, repeating the whole process until convergence is achieved.

4.2 Optimal relaxation parameter

In order to evaluate an optimal relaxation parameter, the following square error functional is here minimized:

$$f(\phi) = \; ||\,\mathbf{U}_N^{b\,(k+1)}(\phi) - \mathbf{U}_N^{b\,(k)}(\phi)||^2, \tag{23}$$

Taking into account the relaxation of the prescribed values for the $(k+1)$ and (k) iterations, equations (24a) and (24b) may be written, regarding equation (22):

$$\mathbf{U}_N^{b\,(k+1)} = (\phi)\mathbf{U}_N^{b\,(k+\phi)} + (1-\phi)\mathbf{U}_N^{b\,(k)}, \tag{24a}$$

$$\mathbf{U}_N^{b\,(k)} = (\phi)\mathbf{U}_N^{b\,(k+\phi-1)} + (1-\phi)\mathbf{U}_N^{b\,(k-1)}. \tag{24b}$$

Substituting equations (24) into equation (23) yields:

$$\begin{aligned} &f(\phi) = ||\,(\phi)\mathbf{W}^{(k+\phi)} + (1-\phi)\,\mathbf{W}^{(k)}||^2 = \\ &= (\phi^2)||\,\mathbf{W}^{(k+\phi)}||^2 + 2\phi(1-\phi)\,(\mathbf{W}^{(k+\phi)}, \mathbf{W}^{(k)}) + (1-\phi)^2||\,\mathbf{W}^{(k)}||^2 \quad , \end{aligned} \tag{25}$$

where the inner product definition is employed (e.g.,$(\mathbf{W},\mathbf{W}) = \; ||\,\mathbf{W}||^2$) and new variables, as defined in equation (26), are considered.

$$\mathbf{W}^{(k+\phi)} = \mathbf{U}_N^{b\,(k+\phi)} - \mathbf{U}_N^{b\,(k+\phi-1)}. \tag{26}$$

To find the optimal ϕ that minimizes the functional $f(\phi)$, equation (25) is differentiated with respect to ϕ and the result is set to zero, as described below:

$$(\phi)||\,\mathbf{W}^{(k+\phi)}||^2 + (1-2\phi)\,(\mathbf{W}^{(k+\phi)}, \mathbf{W}^{(k)}) + (\phi-1)||\,\mathbf{W}^{(k)}||^2 \; = 0. \tag{27}$$

Re-arranging the terms in equation (27), yields:

$$\phi = (\mathbf{W}^{(k)}, \mathbf{W}^{(k)} - \mathbf{W}^{(k+\phi)}) / ||\mathbf{W}^{(k)} - \mathbf{W}^{(k+\phi)}||^2, \tag{28}$$

which is an easy to implement expression that provides an optimal value for the relaxation parameter ϕ, at each iterative step.

It is important to note that expression (28) is deduced by a minimization of an error functional (see equation (23)), which describes the result discrepancies along the common interfaces at each iterative step. Several other methodologies may be considered in order to try to achieve an optimal relaxation parameter, some being quite computationally demanding (see Elleithy Al-Gahtani and El-Gebeily (2001), for instance). The main advantage of expression (28) is its low computational cost and, as is described in the section that follows, its good performance.

It is also important to observe that, since a frequency domain analysis is being performed, equation (28) computes a complex number to represent the relaxation parameter. Although this complex number computation could be ranged (e.g., imposing $|\phi| \leq 1$), the authors have observed that faster convergence is usually achieved in the iterative process if a non-restricted relaxation parameter selection, followed by equation (28), is considered. For the first iterative step, a real value of $\phi = 0.5$ is considered here for the relaxation parameter.

5 Numerical analyses

To better understand the behavior of the iterative coupling strategy and of the two described methods (MFS and KM), two test problems are analyzed here. To allow assessing the accuracy of the computed results, the chosen scenarios correspond to systems in which the solid medium is composed of one or more circular inclusions, filled with a homogeneous elastic material, and for which accurate reference results can be used for comparison purposes. In all tests, the fluid medium is assumed to be water, with a density of 1000 kg/m^3 and allowing sound waves to travel at 1500 m/s, while two different solid materials are considered, with the properties described in Table 1.

Table 1: Elastic properties of the solid media.

	ρ (kg/m^3)	E (GPa)	ν
Solid 1	2400.0	30.0	0.2
Solid 2	7000.0	200.0	0.3

5.1 Test case 1 – solid circular inclusion

To initially assess the behavior of the proposed strategies, consider a circular inclusion with unit radius and made of an elastic material, submerged within a fluid medium at position (0.0; 0.0), subject to the effect of a pressure source located at (-2.0; 0.0). This system is first modeled making use of 30 boundary points for the fluid medium (modeled using the MFS) and 50 boundary points for the solid medium (with a total of 226 nodes being used for the KM), as illustrated in Figure 1. The response of this system has been computed at a receiver point, located at (1.0; 1.0), for two different properties of the solid medium (corresponding to Solid 1 and Solid 2), and the corresponding results are depicted in Figure 2; in these calculation, a constant free parameter c = 1.0 was used for KM, while the virtual sources in the MFS are placed 0.3 m away from the interface. The pressure response at the receiver is displayed in Figures 2a1 and 2a2 together with the analytical solution calculated for this problem, making use of the expressions defined in Godinho, Tadeu and Branco (2004); observing these results, it is clear that there is an excellent match between the analytical solution and the numerical calculation performed making use of the iterative coupling procedure between the KM and the MFS.

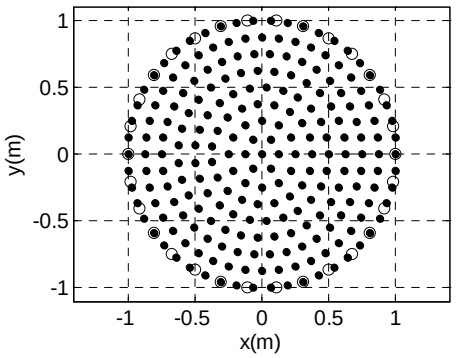

Figure 1: Sketch of the point distribution for the coupled meshless numerical approach, using 30 boundary nodes for the MFS (◯) and 50 boundary nodes (total of 226 nodes) for the KM (●).

To have a better picture of the accuracy associated with this calculation, the error along the coupling interface was calculated for each frequency; this parameter was calculated as the maximum relative error at a set of 50 points uniformly placed along the interface. In plots 2b1 and 2b2, two error curves are displayed, corresponding to calculations performed making use of two different point distributions:

the first corresponds to the one described before, with 50 boundary points for the KM and 30 for the MFS, and in which the boundary nodes of the two distributions do not match; the second corresponds to a situation in which coincident nodes are used, with 40 boundary points being defined for both methods. Clearly, the two curves in each plot follow similar trends, although smaller error levels are observable when a higher number of points is used for the KM. This is expected, since the KM is usually less accurate than the MFS, being necessary a higher number of points in the sub-domains discretized by the KM in order to keep a more uniform error distribution along the model (highlighting the importance of coupling methodologies that allow independent discretizations within each sub-domain). It can also be seen in these curves that the error progressively increases with the frequency, a trend which was expected since the number of points was kept constant for all frequencies. However, for very low frequencies, higher errors are also registered, especially when Solid 2 is modeled. This effect can be due to the fixed value of the free parameter used in this first analysis.

In Figures 2c1 and 2c2, the total number of iterations required to reach convergence at the iterative process is displayed, for the two solids and for the two point distributions described before. It is interesting to note that the number of iterations is always relatively low, reaching a maximum peak of 42 for Solid 1 and for coincident nodes; despite the occurrence of small peaks, the behavior of the presented curves is essentially the same for the two point distributions. It can be noted, however, that the properties of the solid inclusion play an important role in the convergence rate of the iterative process, with significantly fewer iterations being required when Solid 2 is modeled. This is probably due to the fact that Solid 2 exhibits higher Young modulus and mass density, and consequently a weaker solid-fluid interaction develops.

To understand the importance of calculating optimal relaxation parameters in the iterative process, the same analysis was performed for Solid 1 considering fixed values for the relaxation parameter (values of 0.3 and 0.7 are selected). Figure 3 depicts these results, evidencing that when a fixed value is ascribed to the parameter, convergence is not reached within 250 iterations for some frequencies (particularly higher frequencies). This effect clearly reveals how important it is to use an optimization strategy for the calculation of the relaxation parameter. For the frequencies in which convergence was attained with fixed values of the relaxation parameter, accurate results were computed (see Figure 3b). To further reinforce the importance of calculating an optimal relaxation parameter, its variation throughout the iterative process can be analyzed in Figure 4. In this figure, results calculated for three specific frequencies (500 Hz, 1000 Hz and 2000 Hz) along the solid-fluid interface are displayed. For these frequencies, the superposition with the analyt-

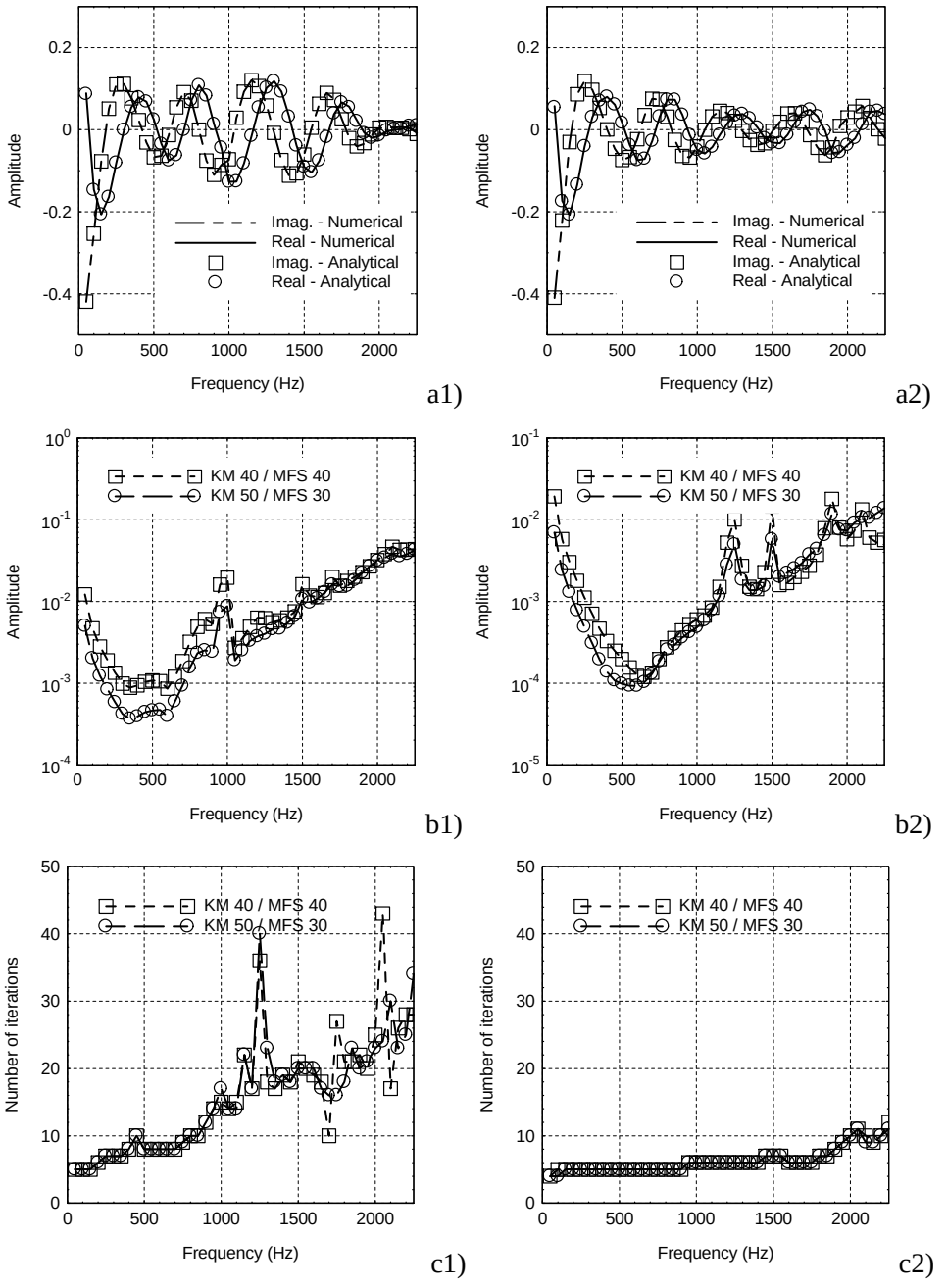

Figure 2: Numerical results in terms of real and imaginary response (a), maximum relative error with respect to the analytical solution computed along the boundary (b), and required number of iterations for convergence, when using two point distributions, and along the frequency domain; in (1) the elastic medium is considered to be Solid 1, while in (2) Solid 2 is assumed.

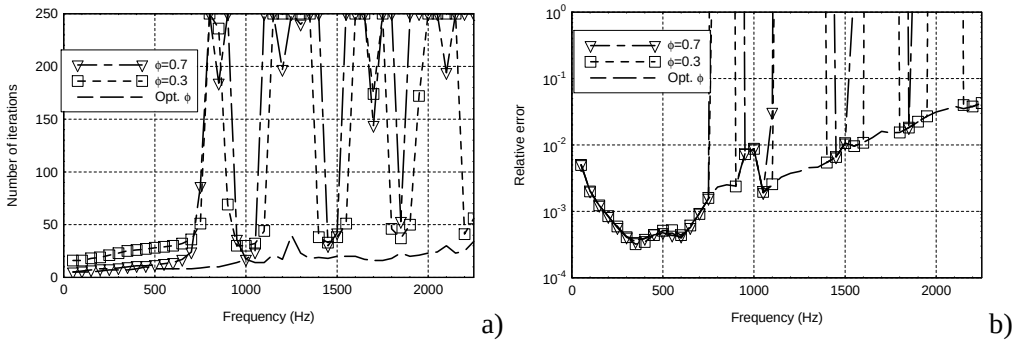

Figure 3: Number of iterations required for convergence (a) and maximum relative error along the boundary (b) when using an optimized versus a constant relaxation parameter, calculated for the case of Solid 1, using 50 boundary nodes for the KM and 30 boundary nodes for the MFS, and using $c = 1.0$.

ical results reveals an excellent agreement, as can be confirmed in Figures 4a1, 4b1 and 4c1. In Figures 4a2, 4b2 and 4c2 the evolution of the real and imaginary components of the relaxation parameter throughout the iterative process is plotted, revealing that it is indeed iteration-dependent, and exhibits strong variations.

A separate convergence analysis of the two methods (KM and MFS) was also conducted, and is presented in Figures 5 and 6. In Figure 5, a fixed number of 60 boundary points is used for the MFS; as for the KM, an initial point distribution with 16 points (considering both the boundary and internal points) is considered, and is then progressively refined, up to a maximum of 850 points. Results are displayed in Figure 5a for the same three frequencies analyzed before, and it can be seen that, for all of them, the response progressively improves towards the correct solution. As expected, better results are computed for the lower frequencies, since, for those frequencies, the same total number of points corresponds to a larger number of points per wavelength. It should be mentioned that the convergence rate depicted in the figure is, in fact, very good, being better than those usually observed with classical numerical methods such as the FEM (Finite Element Method) or the FDM (Finite Difference Method). Additionally, in Figure 5b the total number of iterations required for each point distribution and for each frequency is also presented. Although some variability is observable for the higher frequency, the total number of iterations is always small, and never exceeds 45. A similar study was performed for the MFS point distribution, making use of a fixed point distribution for the KM (with 50 boundary points), and starting with just 10 MFS boundary points. The results are presented in Figure 6, and reveal a progressive improve-

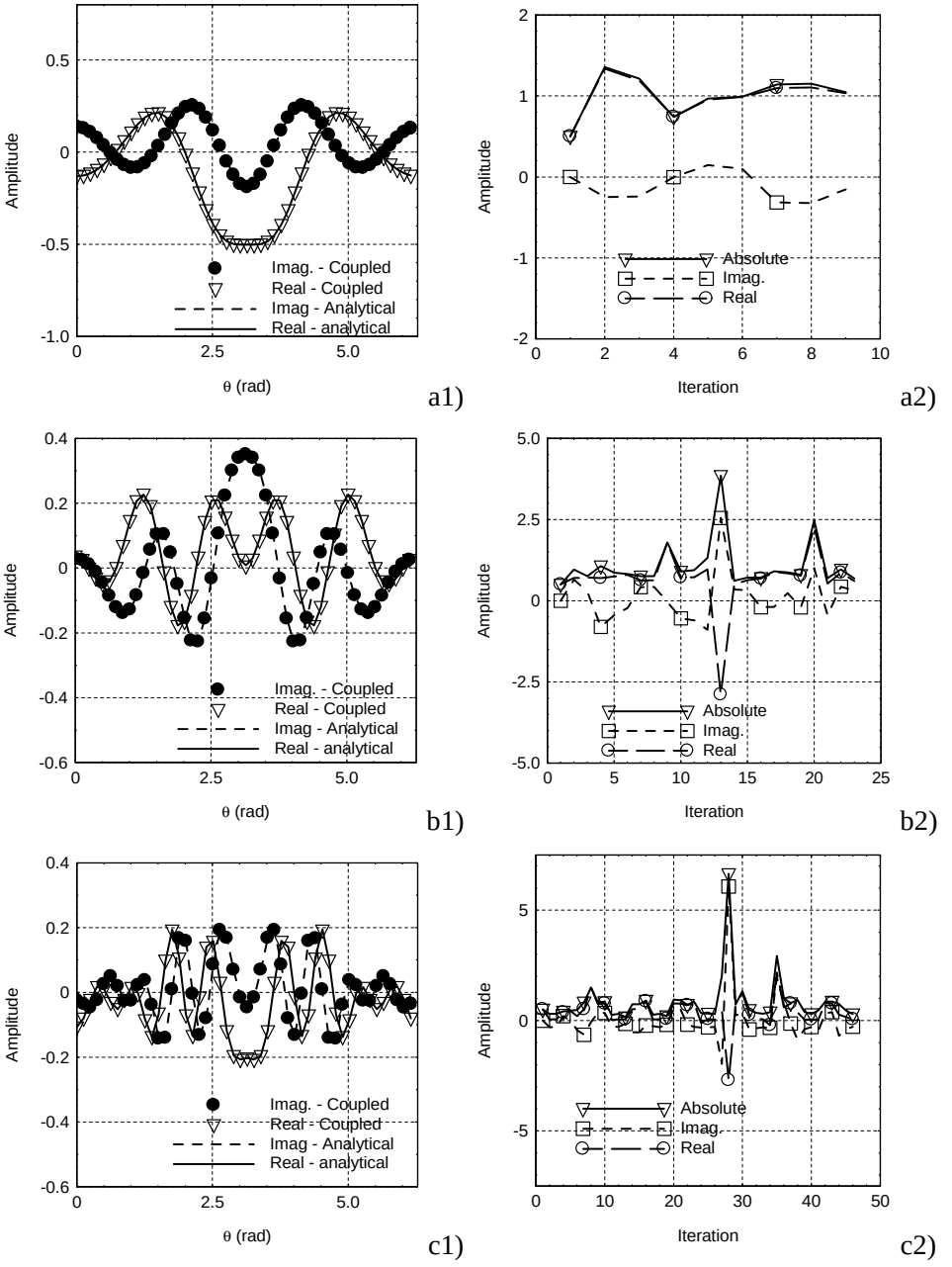

Figure 4: Behavior of the coupling algorithm at specific frequencies of 500 Hz (a), 1000 Hz (b) and 2000 Hz (c), when c= 1.0 and using 30 boundary nodes for the MFS, and 50 boundary nodes for the KM. In (a1,b1,c1), the analytical and the numerical responses along the boundary are shown; in (a2,b2,c2) the evolution of the relaxation parameter along the iterative process is depicted.

ment of the solution as the number of points is increased. However, a frequency-dependent saturation level of the relative error is reached at some point, indicating that above this point the solution quality is being controlled by the KM. As before, although the number of iterations exhibits some variability (see Figure 6b), the number of iterations is always well-controlled.

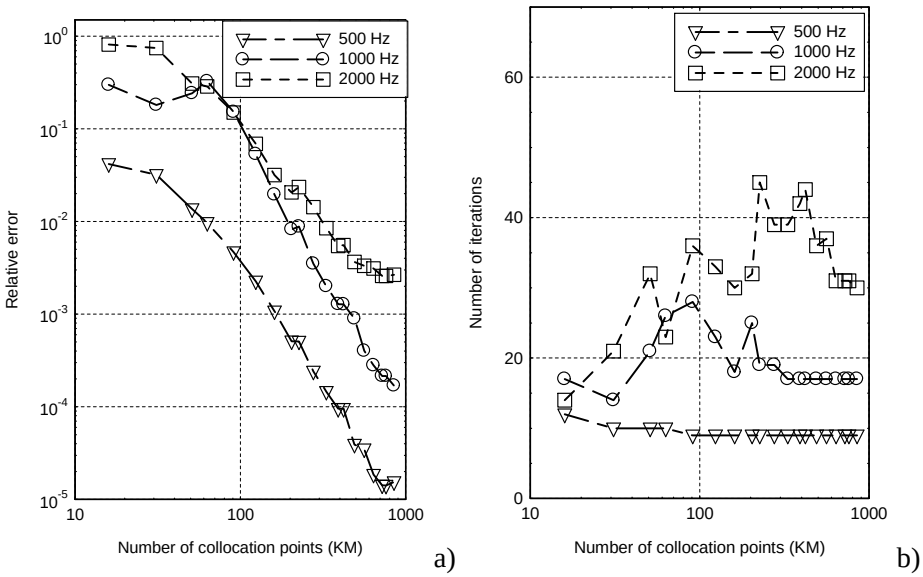

Figure 5: Results computed for frequencies of 500 Hz, 1000 Hz and 2000 Hz when $c = 1.0$ using 60 boundary points for the MFS: a) Convergence curves representing the relative error as a function of the number of KM collocation points; b) Number of iterations for convergence, as a function of the number of KM collocation points.

A final parametric study was conducted to have some insight on the behavior of the KM as a function of its free-parameter c. Thus, a full range of c values was considered (from 0.2 to 4.0, with increments of 0.2), and the maximum relative error along the interface was evaluated for each of them. In an initial approach, the KM problem is solved using a Gaussian solver; for that case, Figures 7a, 7b and 7c reveal that the response steadily improves up to a certain value of c, and then suddenly degrades. Although some frequency-dependence is observed, the limit value of c is always between 1.2 and 1.6, after which the response gets considerably worse. To better understand this behavior, the KM system condition number was calculated for each case, and is depicted in Figure 7d. As expected, this number grows with the increase in the values of c, and around $c = 1.8$ reaches very high values (around 10^{21}), indicating a very ill-conditioned system; indeed, the ill-

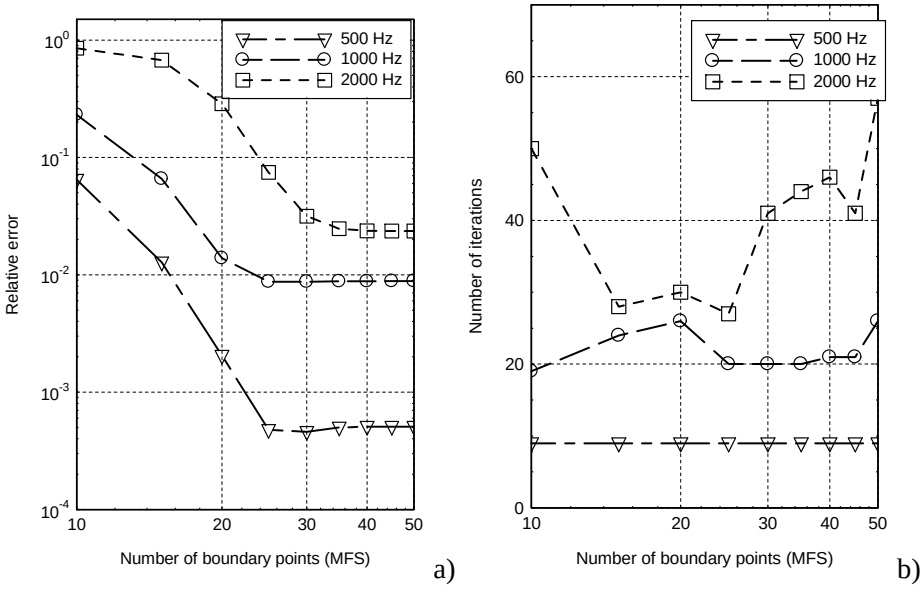

Figure 6: Results computed for frequencies of 500 Hz, 1000 Hz and 2000 Hz when $c = 1.0$ using 50 boundary points for the KM: a) Convergence curves representing the relative error as a function of the number of MFS boundary points; b) Number of iterations for convergence, as a function of the number of MFS boundary points.

conditioning is a known cause of problems in the KM (see, for example, Kansa and Hon (2000)), which is responsible for the degradation of the response for higher c values. In an attempt to help circumventing this problem, the use of an SVD solver was also addressed, and the calculated curves are included in Figures 7a, 7b and 7c. Clearly, this solver can help in the stabilization of the solution, allowing higher values of c to be used with accurate results; however, particularly for the higher frequency, it is not sufficient to guarantee that good results are obtained for high values of c. Although this ill-conditioning issue has been addressed in multiple works, and for several physical problems, for the case of elastodynamic problems very few information is presently available in the literature.

5.2 Test case 2 – multiple solid inclusions in a fluid half-space

One particularly interesting application of the proposed iterative scheme corresponds to the case in which multiple separate solid sub-domains are present within a host fluid medium. Indeed, for this case, application of a direct coupling strategy implies forming very large system matrices, incorporating simultaneously the con-

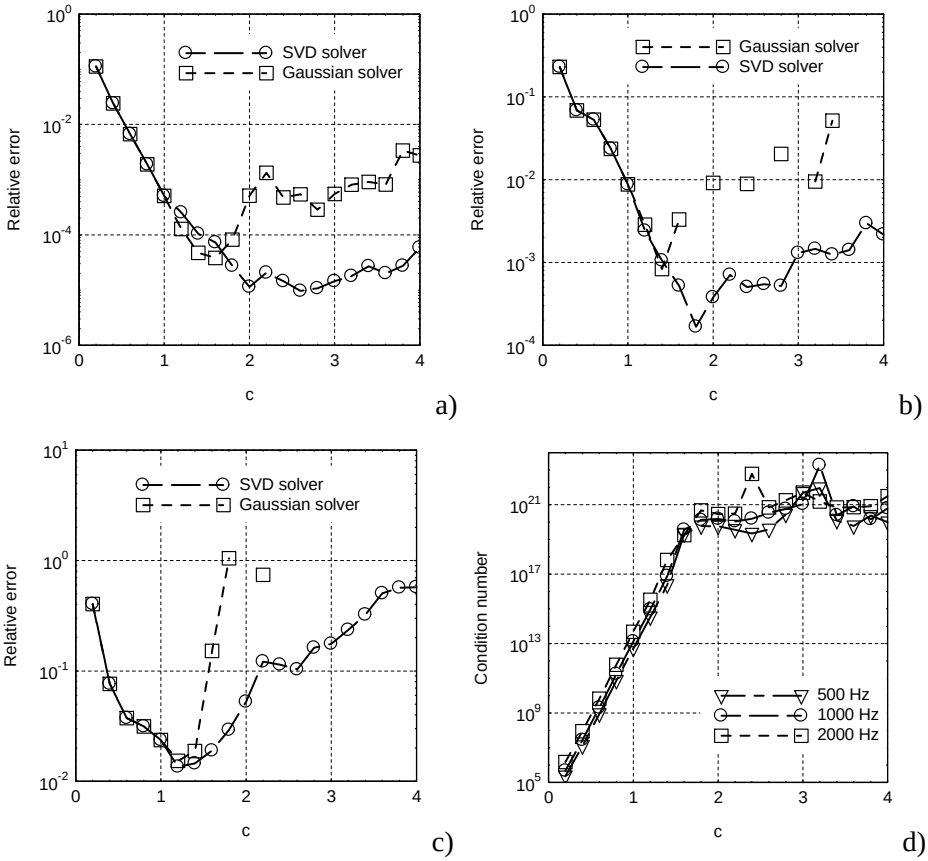

Figure 7: Behavior of the coupled approach for varying values of the shape parameter c: a) Maximum relative error at the boundary for 500 Hz; b) Maximum relative error at the boundary for 1000 Hz; c) Maximum relative error at the boundary for 2000 Hz; d) Condition number of the KM system for the analyzed frequencies. In (a), (b) and (c), missing points correspond to values of the free parameter for which convergence was not reached. 40 boundary nodes were used for the MFS, and 50 boundary nodes were used for the KM.

tribution of all sub-domains. By portioning the problem, and separately analyzing each solid sub-domain and the host fluid, a much more efficient implementation can be obtained, requiring considerably fewer computational resources.

To illustrate this application, consider a physical system consisting of a half-space fluid medium (which is here assumed, once again, to be water) within which four circular solid inclusions are embedded. The material composing these inclusions

is assumed to have the properties of Solid 1, each inclusion having a unit radius, and the system is illuminated by an acoustic source positioned at (-2.0; 5.0). The numerical model defined for the analysis of this problem is based on the application of the KM with 50 boundary nodes and a total of 226 nodes for each inclusion, and of the MFS with 30 boundary nodes to define each inclusion. This configuration is schematically represented in Figure 8. In what follows, and given the results obtained in the previous section, a constant value of the free parameter c=1.0 is used for KM, and the virtual sources of the MFS are positioned at a distance of 0.3 m from the boundary of each inclusion.

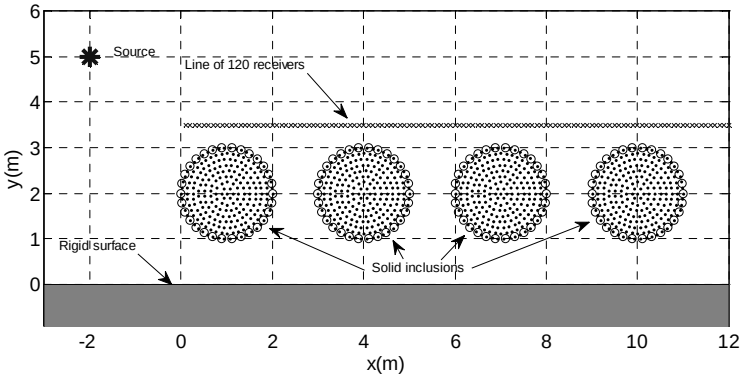

Figure 8: Sketch of the model for the second test problem, including the point distribution for the coupled numerical approach. For each inclusion, 30 boundary nodes are used in the MFS (◯), and 50 boundary nodes (total of 226 nodes) are used in the KM (•). The solid inclusion is assumed to have the properties of Solid 1.

Figure 9 illustrates the results calculated using the proposed model at a receiver positioned at (6.0; 3.5), for 128 frequencies ranging from 5 Hz to 640 Hz. In Figure 9a, the real and imaginary components of the pressure response are illustrated, plotting the numerical results calculated using the proposed coupled approach together with a reference solution calculated using the hybrid analytical-numerical strategy proposed by Godinho, Amado-Mendes and Pereira (2011). As can be seen in the figure, the responses agree very well, with the results provided by the KM-MFS approach following the reference results throughout the frequency domain. In Figure 9b, the required number of iterations for the iterative process to converge, at each frequency, is plotted. As can be seen, a maximum of around 70 iterations is required for the frequency of 10 Hz, and this number then lowers to around 20 iterations. For the higher frequencies, above 600 Hz, the number of iterations in-

creases and, in that range, around 50 iterations are required for convergence. These numbers reveal that the required number of iterations is relatively small, with the iterative process revealing a good convergent behavior. To once again demonstrate the importance of using an optimized relaxation parameter, the same calculation was also performed making use of a constant relaxation parameter with value of 0.5. The corresponding results, in terms of the number of iterations, are also shown in Figure 9b. Clearly, the use of optimal relaxation parameters always leads to a better convergence of the algorithm. Additionally, for some frequencies, convergence is not reached with a fixed relaxation parameter, and the use of optimized parameters is necessary for that purpose.

To verify the accuracy of the approach in the spatial domain, the response was also computed at a number of receiver points located in the fluid, between x=0.0 and x=12.0. Figure 10 illustrates the calculated results for frequencies of 100 Hz, 500 Hz and 640 Hz. For all cases, a reference solution computed making use of the hybrid approach described by Godinho, Amado-Mendes and Pereira (2011) is also displayed. Indeed, for the three analyzed frequencies, both the real and the imaginary parts of the response calculated by the two methods coincide for the full set of receivers. To give some more insight on the iterative process for these frequencies, the evolution of the optimal value of the relaxation parameter is presented in Figure 11. As can be seen in Figures 11a, 11b and 11c, a strong variation of this parameter can occur between consecutive iterations, with absolute values ranging from 0 to 6.

As mentioned at the beginning of this section, one of the most significant advantages of performing a separated analysis of each sub-domain is that the resulting matrices are of reduced size and can be handled with more simplicity. For the present case, the solution of the problem making use of the iterative process requires, for each frequency, assembling 4 matrices (one for each solid sub-domain) for the KM, each of them being a square matrix with $(226\text{x}2)^2=452^2$ entries, and one matrix for the MFS, with $(30\text{x}4)^2=120^2$ entries; given the nature of the involved methods, these are fully populated matrices. If the problem was to be solved by means of a direct coupling between the two numerical methods, a very large system with $(226\text{x}2\text{x}4)^2=1808^2$ entries would be required, keeping the same discretization for the KM sub-domains and improving the discretization of the MFS sub-domain (which already implicates in a more demanding computational procedure), in order to have matching nodes at the common interfaces (as it has been described along this work, the discretization of the KM sub-domain is dominant for the accuracy of the methodology). In this case, taking into account standard direct solvers for instance, savings in computational costs are substantial, since additional triangular solutions cost only $O(n^2)$ work, in contrast to $O(n^3)$ cost of fac-

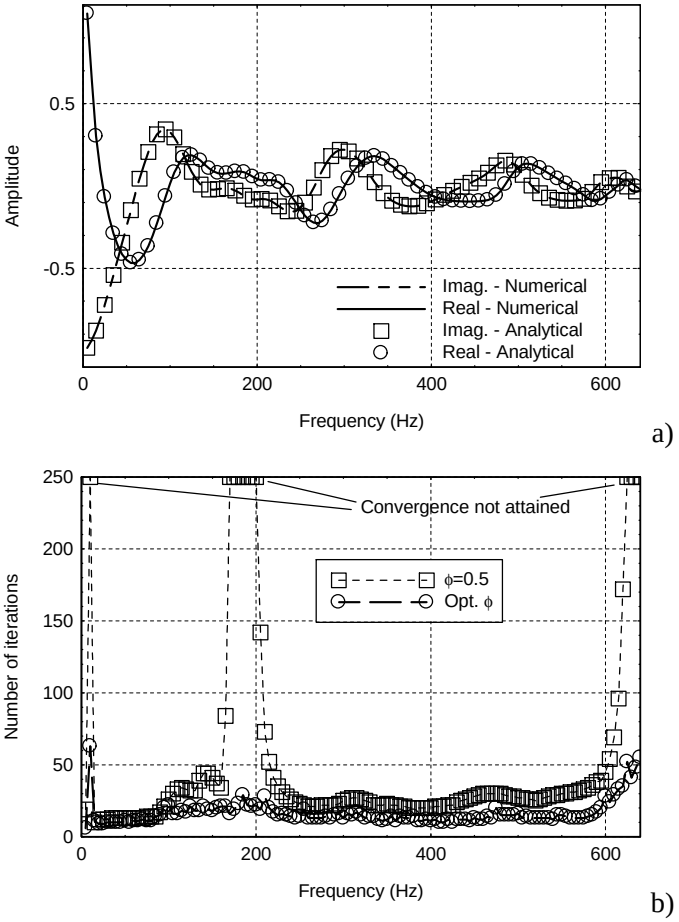

Figure 9: Behavior of the response at the receiver placed at x=6.0 m and y=3.5 m for frequencies ranging from 5 Hz to 640 Hz. In (a) the real and the imaginary components of the response are shown, while (b) illustrates the number of iterations required at each frequency to attain convergence.

torization. Thus, in this context, for the present application, the cost of the iterative analysis can be represented by $[4O({n_{km}}^3) + O({n_{mfs}}^3)] + m[4O({n_{km}}^2) + O({n_{mfs}}^2)]$, where n_{km} and n_{mfs} stand for the dimension of the KM and MFS matrices, respectively, and m represents the number of iterative steps in the analysis. On the other hand, the cost of the standard direct coupling solution can be represented by $[O({n_{coupled}}^3) + O({n_{coupled}}^2)]$, where $n_{coupled}$ stands for the dimension of the coupled matrix. Since here one has n_{km} = 452, n_{mfs} = 120 and $n_{coupled}$ = 1808, the

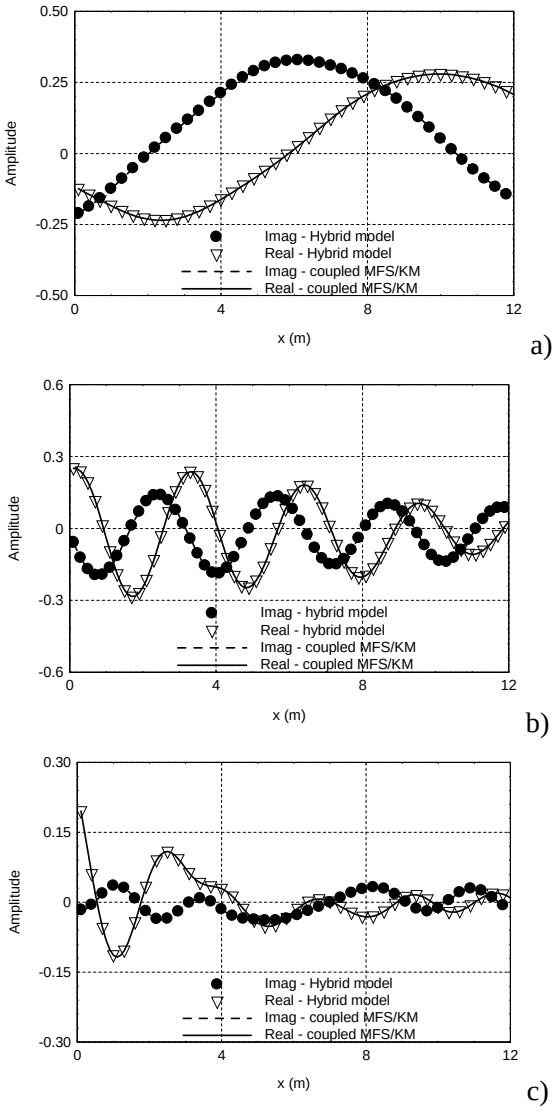

Figure 10: Response for frequencies of 100 Hz (a), 500 Hz (b) and 640 Hz (c) calculated using the proposed approach and the hybrid approach of reference [Godinho, Amado-Mendes and Pereira (2011)], along the line of receivers.

iterative analysis is expected to be more efficient than the standard coupling approach even if more than 6000 iterations are necessary for convergence, which is quite an expressive amount. This obviously leads to very different requirements

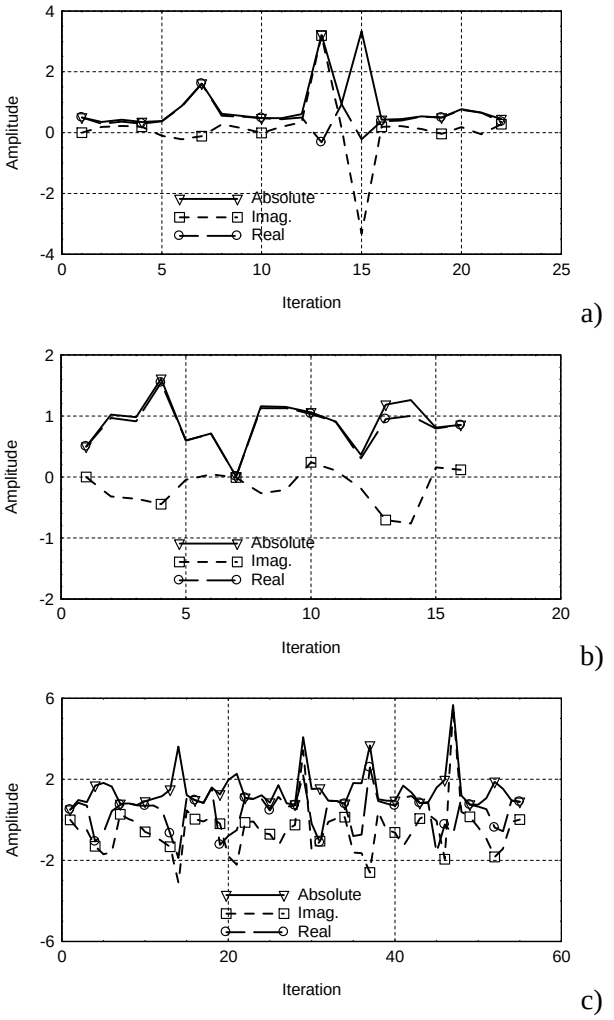

Figure 11: Evolution of the relaxation parameter along the iterative process for frequencies of 100 Hz (a), 500 Hz (b) and 640 Hz (c).

from the computational point of view, with the iterative process being much more efficient for this type of problems.

6 Conclusions

This work proposes an iterative coupling algorithm between the MFS and KM for the analysis of interacting acoustic-elastodynamic problems. The coupled fluid-

solid model is solved in the frequency domain, separately analyzing the acoustic fluid and the elastodynamic solid sub-domains, resulting in simpler and better conditioned systems of equations, improving the accuracy of the methodology. Moreover, by performing the separate analysis of the two media, large savings in computational resources can be made, and the proposed strategy may become much more efficient than standard direct coupling approaches. The iterative coupling is also more flexible, easily allowing the adoption of totally independent discretizations for each sub-domain, not requiring matching nodes at common interfaces. As a consequence, only interface routines are required when one wishes to use existing codes to build coupling algorithms, taking full advantage of specialized features and disciplinary expertise built into single-field models.

As it was discussed along the paper, the effectiveness of the iterative coupling algorithm is closely related to the introduction of relaxation parameters in the analyses. In this work, an efficient and easy to implement expression to compute optimal values for the relaxation parameter, at each iterative step, is presented, considerably improving the performance and the robustness of the methodology. As a matter of fact, acoustic-elastodynamic iterative coupled analyses in the frequency domain are well-known ill-posed problems, and the introduction of optimal relaxation parameters was able to properly deal with this complex numerical drawback, allowing convergence to be usually obtained at few iterative steps.

Although the coupling of meshless formulations was focused here, the discussed iterative coupling algorithm is generic, and can be easily applied considering the coupling of any numerical method, more properly dealing with the specific physical and geometrical characteristics of the sub-domains of the coupled model. The framework presented here is very appropriate to analyze problems where adaptive discretization techniques are required (which is intended as future works). In this case, the renewal of point distribution can be carried out within the iterative steps of the coupling solution, taking full advantage of the geometrical flexibility of the meshless formulations and of the independent sub-domains solution.

Acknowledgement: The first author acknowledges the financial support by FCT (Fundação para a Ciência e Tecnologia, Portugal), in the scope of project PTDC-/ECM/114505/2009. The financial support by CNPq (Conselho Nacional de Desenvolvimento Científico e Tecnológico) and FAPEMIG (Fundação de Amparo à Pesquisa do Estado de Minas Gerais) is greatly acknowledged by the second author.

References

Belytschko, T.; Geers, T.L. (eds.) (1977). *Computational methods for fluid-structure interaction problems*. AMD vol.26, American Society of Mechanical Engineers, New York.

Benamou, J.D.; Despres, B. (1997). A domain decomposition method for the Helmholtz equation and related optimal control problems. *Journal of Computational Physics*, 136: 68-82.

Cho, H.; Golberg; M., Muleshkov A.; Li X. (2004). Trefftz Methods for time dependent partial differential equations. *CMC:Computers, Materials and Continua*, 1: 1–38.

Czygan, O.; von Estorff, O. (2002). Fluid-structure interaction by coupling BEM and nonlinear FEM. *Engineering Analysis with Boundary Elements*, 26**:** 773-779.

Elleithy, W.M.; Al-Gahtani, H.J.; El-Gebeily, M. (2001). Iterative coupling of BE and FE methods in elastostatics. *Engineering Analysis with Boundary Elements*, 25: 685–695.

Fairweather, G.; Karageorghis, A. (1998). The method of fundamental solutions for elliptic boundary value problems. *Advances in Computational Mathematics*, 9: 69–95.

Farhat, C.; Lesoinne, M.; LeTallec, P. (1998). Load and motion transfer algortihms for fluid/structure interaction problems with non-matching discrete interfaces: momentum and energy conservation, optimal discretization and application to aeroelasticity, *Computer Methods in Applied Mechanics and Engineering*, 157: 95-114.

Fasshauer, G.E.; Zhang, J.G. (2007). On choosing "optimal" shape parameters for RBF approximation. *Numerical Algorithms*, 45, 1–4: 345–368.

Godinho, L.; Amado Mendes, P.; Pereira, A. (2011). A hybrid analytical-numerical model based on the method of fundamental solutions for the analysis of sound scattering by buried shell structures. *Mathematical Problems in Engineering*, 2011, Article ID 710623, 22 pages. doi:10.1155/2011/710623.

Godinho, L.; Tadeu, A.; Branco, F. (2004). Dynamic analysis of submerged fluid-filled pipelines subjected to a point pressure load. *Journal of Sound and Vibration*, 271, 1-2: 257-277.

Golberg, M.A.; Chen, C.S. (1999). The method of fundamental solutions for potential, Helmholtz and diffusion problems. In *Boundary Integral Methods: Numerical and Mathematical Aspects*. Golberg MA (ed.). WIT Press & Computational Mechanics Publications, Boston, Southampton: 103–176.

Kansa, E. (1990a). Multiquadrics A scattered data approximation scheme with

applications to computational fluiddynamics I surface approximations and partial derivative estimates. *Computers & Mathematics with Applications*, **19**: 127–145.

Kansa, E. (1990b). Multiquadrics - A scattered data approximation scheme with applications to computational fluiddynamics II solutions to parabolic, hyperbolic and elliptic partial differential equations. *Computers & Mathematics with Applications*, **19**: 147–161.

Kansa, E.; Hon, Y.C. (2000). Circumventing the ill-conditioning problem with multiquadric radial basis functions: Applications to elliptic partial differential equations. *Computers & Mathematics with Applications*, 39: 123-137.

Lie, S.T.; Yu, G.Y.; Zhao, Z. (2001). Coupling of BEM/FEM for time domain structural-acoustic interaction problems. *CMES: Computer Modeling in Engineering & Sciences*, 2: 171-180.

Lin, C.C. (1996). An iterative finite element-boundary element algorithm. *Computers & Structures*, 59: 899-909.

Lombard, B.; Piraux, J. (2004). Numerical treatment of two-dimensional interfaces for acoustic and elastic waves, *Journal of Computational Physics*, 195: 90-116.

Maman, N.; Farhat, C. (1995). Matching fluid and structure meshes for aeroelastic computations: a parallel approach. *Computer & Structures*, 54: 779-785.

Mathews, I.C. (1986). Numerical techniques for three-dimensional steady-state fluid-structure interaction. *Journal of the Acoustical Society of America*,79: 1317-1325.

Park, K.C.; Felippa, C.A.; Ohayon, R. (2001). Partioned formulation of internal fluid-structure interaction problems via localized Lagrange multipliers. *Computer Methods in Applied Mechanics and Engineering*, 190: 2989-3007.

Sarra, S.A.; Sturgill, D. (2009). A random variable shape parameter strategy for radial basis function approximation methods. *Engineering Analysis with Boundary Elements*, 33: 1239–1245.

Soares, D.; von Estorff, O.; Mansur, W.J. (2004). Iterative coupling of BEM and FEM for nonlinear dynamic analyses. *Computational Mechanics*, 34, 1: 67-73.

Soares, D.; von Estorff, O.; Mansur, W. (2005). Efficient non-linear solid-fluid interaction analysis by an iterative BEM/FEM coupling. *International Journal for Numerical Methods in Engineering*, 64, 11: 1416–1431.

Soares, D.; Mansur; W. J.; Lima, D.L. (2007). An explicit multi-level time-step algorithm to model the propagation of interacting acoustic-elastic waves using finite element/finite difference coupled procedures. *CMES: Computer Modeling in Engineering and Sciences*, 17, 1: 19–34.

Soares, D. (2008). A time-domain FEM-BEM iterative coupling algorithm to numerically model the propagation of electromagnetic waves. *CMES: Computer Modeling in Engineering and Sciences*, 32: 57-68.

Soares, D. (2009). Fluid-structure interaction analysis by optimised boundary element-finite element coupling procedures. *Journal of Sound and Vibration*, 322, 1-2: 184–195.

Soares, D. (2011). Coupled numerical methods to analyze interacting acoustic-dynamic models by multidomain decomposition techniques. *Mathematical Problems in Engineering*, 2011: 1-28.

Soares, D. (2012). FEM-BEM iterative coupling procedures to analyze interacting wave propagation models: fluid-fluid, solid-solid and fluid-solid analyses. *Coupled Systems Mechanics*, 1: 19-37.

Soares, D.; Godinho, L.; Pereira, A.; Dors, C. (2012). Frequency-domain analysis of acoustic wave propagation in heterogeneous media considering iterative coupling procedures between the Method of Fundamental Solutions and the Kansa's Method. *International Journal for Numerical Methods in Engineering*, **89**, 7: 914-938.

Tadeu, A.; Godinho, L.; Chen, C.S. (2005). Performance of the BEM, MFS, and RBF collocation method in a 2.5D wave propagation analysis. *WIT transactions on modelling and simulation*, 39: 143:153.

von Estorff, O.; Antes, H. (1991). On FEM-BEM coupling for fluid-structure interaction analysis in the time domain. *International Journal for Numerical Methods in Engineering*, 31: 1151-1168.

Warszawski, A.; Soares, D.; Mansur, W.J. (2008). A FEM-BEM coupling procedure to model the propagation of interacting acoustic-acoustic/acoustic-elastic waves through axisymmetric media. *Computer Methods in Applied Mechanics and Engineering*, 197, 45–48: 3828–3835.

Yan, B.; Du, J.; Hu, N. (2006). A domain decomposition algorithm with finite element-boundary element coupling. *Applied Mathematics and Mechanics – English edition*, 27, 4: 519-525.